Ionization modulation of H by two time-delayed strong IR pulses

Shu-Na Song,[1] Ji-Wei Geng,[1] Li-Zhong Li,[1] Hong-Bing Jiang,[1,*] and Liang-You Peng[1,2,†]

[1]*State Key Laboratory for Mesoscopic Physics and Department of Physics, Peking University, Beijing 100871, China*

[2]*Collaborative Innovation Center of Quantum Matter, Beijing 100871, China*

(Received 15 January 2015; revised manuscript received 24 March 2015; published 1 May 2015)

The ionization modulation of the hydrogen atom is investigated theoretically by the numerical solution to the time-dependent Schrödinger equation and the strong-field-approximation method. Considering a pair of identical but time-delayed one-cycle infrared laser pulses, we find that the total ionization yield is modulated by the time delay between the two pulses. We show that the modulation is mainly due to the interference of electron wave packets in the continuum states respectively generated by each of the two pulses. In this tunneling regime, we identify some similarities to and differences from the usual quantum control of electron transition that is in the perturbation regime. Finally, we also extend our study of ionization modulation to the one-multicycle-laser-pulse case with different wavelengths in the tunneling regime.

DOI: 10.1103/PhysRevA.91.053401 PACS number(s): 32.80.Rm, 42.50.Hz, 42.65.Re

I. INTRODUCTION

Techniques of generating various shaped laser pulses have enabled us to control atomic and molecular dynamics, which is of great importance in physics, chemistry, and biology [1–6]. Optical and quantum control have been studied using pulse-shaping technology in the weak-field regime based on second-order time-dependent perturbation theory. Resonant and nonresonant multiphoton absorptions are manipulated by two time-delayed laser pulses, which lead to interference fringes in the photoelectron spectra and controllable steering quantum systems from an initial state to a desired final state. Experimentalists have combined the phase-locked interferometrically generated pulses with pulse-shaping techniques to study the interplay of optical and quantum-mechanical phases in the multiphoton transition [7–11]. The application of pulse-shaping techniques widely expands the range of quantum control achievements [12].

The ionization and transition processes are significantly affected by the temporal profile of the electric field of the pulse. Therefore, the interference of electron wave packets in the continuum states generated by the two time-delayed laser pulses can also be used as a tool to control the excited-state population and the emitted electron spectrum [13]. The information about the shaped laser pulse can be extracted from the electron spectrum [14]. The interference fringes and the fringe spacing in the photoelectron spectrum are determined by the time delay of the two laser pulses. In Ref. [10], the phase effects in a quantum control experiment on the two-photon transition were studied in detail.

As in strong-field ionization, perturbation theory cannot provide a useful solution [15]. We can study this part with the help of the Keldysh theory. When the photon energy is much smaller than the ionization potential I_p, it can be roughly divided into multiphoton ionization ($\gamma \gg 1$) and tunneling ionization ($\gamma \ll 1$) [16], where the Keldysh parameter $\gamma = \sqrt{I_p/2U_p}$, with U_p being the ponderomotive energy of an electron in the laser field. In this paper we investigate ionization modulation by varying the time delay between two laser pulses and extend this quantum control to the tunneling regime. Our results show that the modulation mode is quite similar to that in the weak field, but the underlying mechanism is different. The ionization yield is modulated by the interference of electron wave packets generated by the time-delayed laser pulses. The modulation amplitude is controlled by the time delay and the relative carrier-envelope phase between the two laser pulses and the modulation period is determined by the ionization potential and the relative carrier-envelope phase. In our time-dependent Schrödinger equation (TDSE) calculations, we use both the Coulomb potential and the Yukawa potential to identify the main modulation mechanism and to find the roles played by the Coulomb potential. For shorter wavelengths, we find the effects of the excited states in the Coulomb potential case [17,18]. We find that the ionization modulation also exists in the one-multicycle-laser-pulse case by varying the wavelength in the tunneling regime. The modulation can be explained by the interference between the electron wave packets generated in different cycles.

The organization of the rest of this paper is as follows. In Sec. II the numerical and analytical method are described in brief. In Sec. III we present our main results and a discussion. Section IV is a short summary.

II. THEORETICAL METHODS

The method is based on the numerical solution to the TDSE, whose details can be found in previous work [19–21]. In this work, the hydrogen in its ground $1s$ state is exposed to two time-delayed linearly polarized short laser pulses, with a combined vector potential given by

$$\begin{aligned}\mathbf{A}_L(t) &= \hat{z}A_{L1}(t) + \hat{z}A_{L2}(t - T_d) \\ &= \hat{z}A_0\{f_L(t)\sin(\omega t) + f_L(t - T_d) \\ &\quad \times \sin[\omega(t - T_d) + \Phi_{CEP}]\}, \end{aligned} \tag{1}$$

where A_0 is the peak value of the vector potential of each pulse, ω is the carrier frequency, and T_d and Φ_{CEP} are, respectively, the time delay and the relative carrier-envelope phase between the two laser pulses. The corresponding electric field is given

*hbjiang@pku.edu.cn

†liangyou.peng@pku.edu.cn

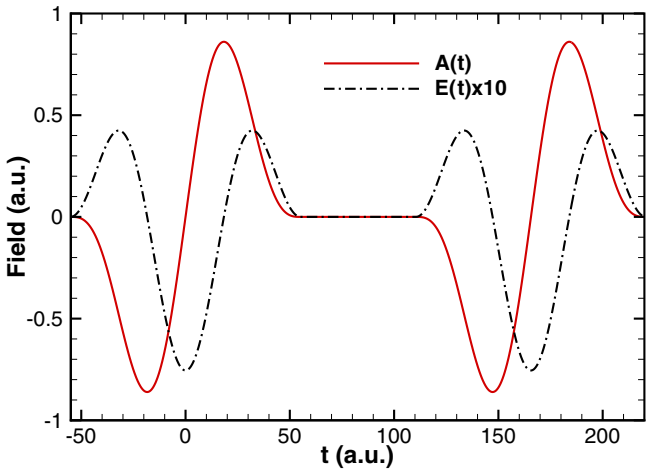

FIG. 1. (Color online) The two time-delayed laser pulses adopted in this work. As an example, both the vector potential and the electric-field strength (multiplied by a factor of 10) are shown for two 800-nm laser pulses at the peak intensity of $I_0 = 2 \times 10^{14}$ W/cm^2 with a time delay of 55.3 a.u.

by $\mathbf{E}_{\rm L}(t) = -\partial \mathbf{A}_{\rm L}(t)/\partial t$. The pulse envelope is given by

$$f_{\rm L}(t) = \cos^2\left(\frac{\pi}{\tau}t\right), \tag{2}$$

with τ the duration of each pulse, which is taken to be one optical cycle. In Fig. 1 we show the vector potential and the electric field for 800-nm laser pulses with a time delay of 55.3 a.u. In the rest of the present work, the peak laser intensity is taken to be 2×10^{14} W/cm^2.

In brief, the TDSE

$$i\frac{\partial}{\partial t}\Psi(\mathbf{r},t) = \left[-\frac{1}{2}\nabla^2 + V(r) + \mathbf{p}\cdot\mathbf{A}_{\rm L}(t)\right]\Psi(\mathbf{r},t) \tag{3}$$

is numerically solved in spherical coordinates with the finite-difference method. Two types of atomic potentials are considered, i.e., $V(r) = -1/r$ for the Coulomb potential case and $V(r) = -Z\frac{e^{-\lambda r}}{r}$ for the Yukawa potential case with $Z = 1.91$ and $\lambda = 1$ to reproduce the ground state energy of the H atom. The differential ionization probability is calculated in the same way as in our previous work [21]; the probability of a photoelectron with an asymptotic momentum $\mathbf{k}$ can be obtained by a projection of the final wave function $\Psi(t_f)$ onto the scattering states of the field-free Hamiltonian, i.e.,

$$P(\mathbf{k}) = P(k,\theta,\varphi) = |\langle\Psi_{\mathbf{k}}^-|\Psi(t_f)\rangle|^2. \tag{4}$$

For the linearly polarized pulse considered in the present work, $P(\mathbf{k})$ has an azimuthal symmetry about φ. The total ionization probability can be then calculated by integrating in momentum space, i.e.,

$$P_{\rm total} = 2\pi\int P(k,\theta,\varphi=0)k\,dk\,d\theta. \tag{5}$$

For the purpose of comparison, we also present the results of the strong-field approximation (SFA) [22,23], which neglects the Coulomb potential effects on the electron's motion after its tunneling. Within the first order of the SFA, the ionization amplitude can be given by

$$M_{\rm SFA}(\mathbf{p}) = -i\int_{-\infty}^{\infty} dt\langle\Psi_{\mathbf{p}}^{\rm V}(t)|\mathbf{r}\cdot\mathbf{E}_{\rm L}(t)|\Psi_0(t)\rangle, \tag{6}$$

where

$$\Psi_{\mathbf{p}}^{\rm V}(t) = (2\pi)^{-3/2}\exp\left(i[\mathbf{p}+\mathbf{A}_{\rm L}(t)]\cdot\mathbf{r} - \frac{i}{2}\int_{-\infty}^{t}[\mathbf{p}+\mathbf{A}_{\rm L}(t')]^2dt'\right) \tag{7}$$

is the Volkov state and $|\Psi_0(t)\rangle$ is the atomic ground state.

III. NUMERICAL RESULTS AND DISCUSSION

In this section we calculate the ionization probability as a function of the time delay for wavelengths of 600, 800, 1200, and 1800 nm at the same intensity of 2×10^{14} W/cm^2. We first carry out the calculations for the Coulomb potential case. To identify the main reasons for the ionization modulation and to find out the effects of the Coulomb potential, we also carry out similar calculations using the Yukawa potential, which only has one bound state. The key point of this paper is to investigate quantum coherent control using two time-delayed laser pulses, so we keep the time delay greater than the laser period to avoid optical interference. Therefore, in the following, the modulation is shown as a function of the time delay $T_{\rm d}$ subtracted by the duration of the single pulse τ, i.e., $T_{\rm d} - \tau$.

A. Coulomb potential case

We first consider the modulation of the ionization probability by varying the time delay between two laser pulses for wavelengths of 600, 800, 1200, and 1800 nm. As the intensity we use is the same for the four wavelengths, the Keldysh parameter γ varies from 1 to 0.3. Figure 2 shows that the ionization probability varies as a function of the shifted time delay $T_{\rm d} - \tau$. The ionization probability increases with increasing the wavelength, which is a common feature in the tunneling regime. For all the cases, the total ionization probability oscillates as a function of the time delay. For Figs. 2(a) and 2(b), in which the Keldysh parameters are larger, the *relative* modulation is larger and also the shape is more irregular, which may be due to multiphoton effects. As we can see, the modulation becomes more regular and the oscillation period is also more uniform with an increase of the wavelength. The period of modulation for 1200 and 1800 nm is quite uniform and almost at the same value, which is about $2\pi/I_{\rm p}$. The modulation amplitude decreases with an increase of the wavelength. To get a quantitative comparison of the constructive or destructive modulation in the two-pulse case, in each panel of Fig. 2 we show a dash-dotted line indicating two times of the ionization probability for a single pulse case. For 600 and 800 nm, we find that the center of the oscillating modulation is above the blue dash-dotted line, while it is below the blue dash-dotted line for the cases of 1200 and 1800 nm. These phenomena can be attributed to the population of Rydberg states in the final states, which is verified in Sec. III B.

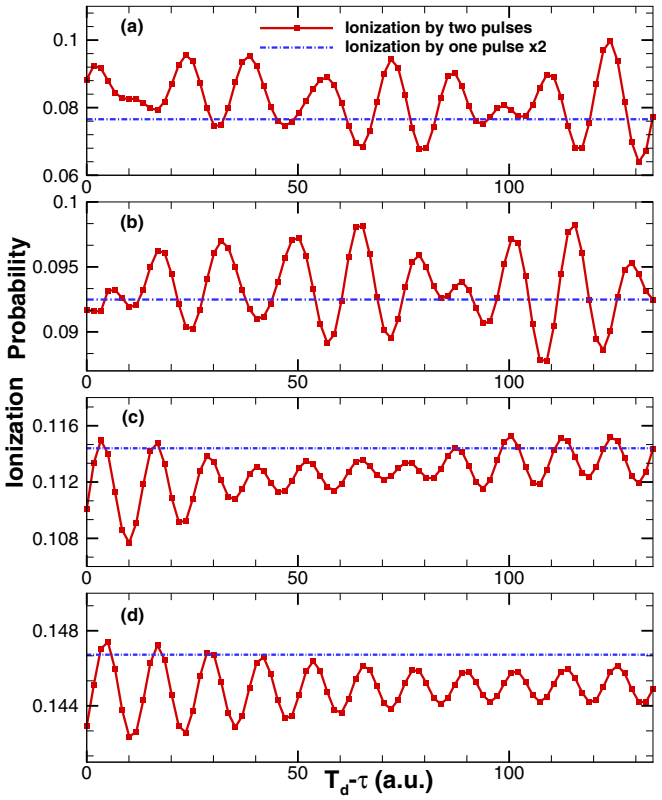

FIG. 2. (Color online) Modulation of the ionization probability as a function of the time delay (shifted by τ), calculated by the TDSE for the case of the Coulomb potential at a fixed peak intensity $I_0 = 2 \times 10^{14}$ W/cm^2 for different wavelengths: (a) 600 nm, $\gamma = 1.0$, (b) 800 nm, $\gamma = 0.75$, (c) 1200 nm, $\gamma = 0.50$, and (d) 1800 nm, $\gamma = 0.34$.

B. Yukawa potential case and SFA simulations

For a Yukawa potential with the parameters we choose, there is only one bound state and there are no effects of excited states or the long-range effects of the Coulomb potential. We can compare with the Coulomb potential to see the effects of the excited states in the ionization modulation. With the same ground state energy, the ionization probability of the Yukawa potential is much smaller than that of the Coulomb potential [24]. We repeat the calculations with the same laser parameters as those in Fig. 2, but for the Yukawa potential case. In Fig. 3(a) we show the ionization modulation as a function of the time delay for the 1800-nm case. We notice that the position of twice the one-pulse ionization probability is just in the center of the oscillation for the two-pulse case. Comparing this with Fig. 2, we conclude that the Rydberg states' population in the final states impacts the constructive or destructive modulation globally. In Fig. 3(b) we show the normalized ionization yield of three wavelengths for the Yukawa potential. We find that, for all three wavelengths, the modulation periods are the same as that in the tunneling regime for the Coulomb potential, which equals $2\pi/I_p$. The modulation shapes of the three wavelength are all very regular, which tells us that the excited states affect the modulation in shorter wavelengths for the Coulomb potential case.

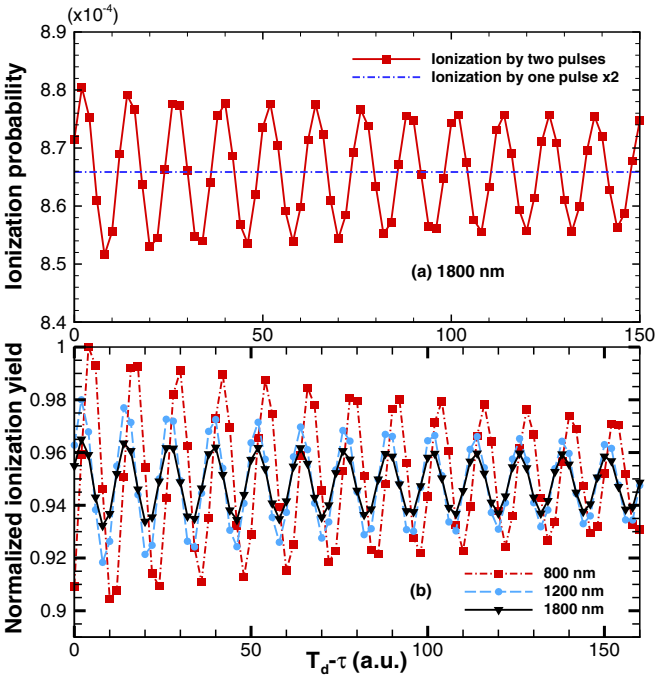

FIG. 3. (Color online) Ionization modulation for the case of the Yukawa potential as a function of the time delay between two laser pulses. (a) The ionization probability (in 10^{-4}) of 1800 nm; (b) The normalized ionization yield of three wavelength. The laser parameters are the same as those in Fig. 2.

There is another similarity to the case of the Coulomb potential, i.e., the modulation amplitude decreases with an increase of the wavelength. For various time delays, we show in Fig. 4 the photoelectron energy spectra along the negative direction of the laser polarization at three different

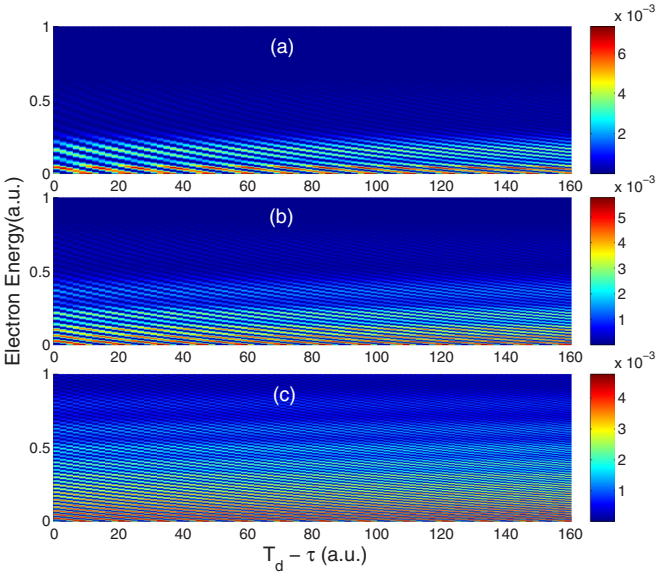

FIG. 4. (Color online) Photoelectron energy distribution along the laser negative polarization direction as a function of time delay between two laser pulses for the Yukawa potential case for (a) 800 nm, (b) 1200 nm, and (c) 1800 nm.

wavelengths (the main signal is in this direction [21]). We notice that the interference fringes become denser with increasing wavelength and time delay. The modulation amplitude decays with an increase of the time delay and wavelength. This shows the general relationship between the modulation amplitude and the density of interference fringes, which has also been discussed in the context of double ionization of He by two time-delayed attosecond pulses [25]. The ionization probability is the integral result of the photoelectron energy spectra and the amplitude of oscillation is smaller when the interference fringes become denser. Note that, in our case, we use the shifted time delay, which is related to the laser wavelength. Therefore, the dependence of the modulation amplitude on the wavelength actually comes from different absolute time delays T_d for different wavelengths.

The above conclusion is quite similar to the case of control of the two-photon absorption induced by two time-delayed laser pulses using the second-order time-dependent perturbation theory. In the weak-field regime, the two-photon transition probability S_2 from the ground state $|g\rangle$ to the final excited state $|f\rangle$ can be described as [26,27]

$$S_2 \propto |a_{\rm opt}(T_d) + a_{\rm QM}(T_d)|^2, \tag{8}$$

with

$$a_{\rm opt}(T_d) = 2\exp\left(-T_d^2/2\tau^2\right)\exp[-i(\omega_{fg}T_d/2 + \Phi_{\rm CEP})] \tag{9}$$

and

$$a_{\rm QM}(T_d) = 1 + \exp[-i(\omega_{fg}T_d/2 + 2\Phi_{\rm CEP})], \tag{10}$$

where ω_{fg} is the transition frequency from the ground state $|g\rangle$ to the final excited state $|f\rangle$ and $a_{\rm opt}(T_d)$ and $a_{\rm QM}(T_d)$ represent the optical and the quantum-mechanical contributions, respectively. In our case, there is only the quantum-mechanical contribution since we have chosen the time delay T_d to be greater than the single-pulse duration τ, so the optical terms does not exist. Thus the two-photon transition probability is periodically modulated by the time delay and the relative carrier-envelope phase $\Phi_{\rm CEP}$ as described in Eq. (10). For a given relative carrier-envelope phase, the modulation period is simply $2\pi/\omega_{fg}$.

If we take the continuum state as the final state, the modulation period of the ionization can be explained by Eq. (10). However, in the tunneling regime where the laser field we use is rather strong, the time-dependent perturbation theory cannot be applied. Nevertheless, the modulation of the ionization yield is the result of interference of free-electron wave packets generated by the two time-delayed laser pulses. If we change the relative carrier-envelope phase $\Phi_{\rm CEP}$ to π, the two electron wave packets will have different momentum distributions at the peak intensity of the laser field and the time intervals of interference will be different from the case of $\Phi_{\rm CEP} = 0$. In this way, the amplitude of the modulation should be decreased and the period can be changed if we change the relative carrier-envelope phase by π. For N-photon ionization in the weak-field case, the phase part in Eq. (10) should be changed as $N\Phi_{\rm CEP}$, so the amplitude and period of the modulation should be the same with $\Phi_{\rm CEP} = \pi$. In Fig. 5 we show the ionization modulation of two relative phases $\Phi_{\rm CEP} =$ 0 and π, taking 1200 nm as an example. The comparison shows that in the strong-field case, the phenomenon is different from

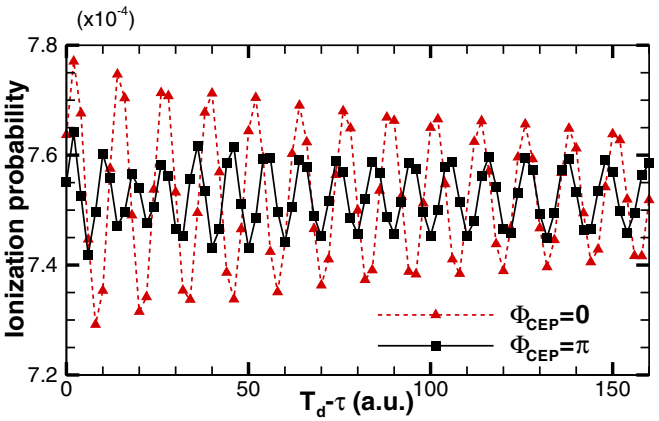

FIG. 5. (Color online) Ionization probability modulation for the Yukawa potential case at two different relative carrier envelope phases for 1200 nm.

the expectation in the weak-field case, although there are some similarities.

To seek a qualitative understanding of the interference, we turn to the SFA. According to the SFA theory, once the electron has entered the continuum it experiences only the laser field and not the atomic binding potential anymore. For the short-range-potential case, it is supposed that the SFA can give results qualitatively similar to those of TDSE calculations. We can achieve a physical picture according to the SFA theory. The electrons generated during the first and second pulses will have different phases,

$$e^{iI_pt_1}e^{-[iE_k(t-t_1)+\varphi_1]} \quad \text{(freed at } t_1\text{)}, \tag{11}$$

$$e^{iI_pt_2}e^{-i[E_k(t-t_2)+\varphi_2]} \quad \text{(freed at } t_2\text{)}, \tag{12}$$

where E_k is the final kinetic energy of the electron and φ_1 and φ_2 represent the phase. When the two electron wave packets have the same momentum, the total ionization probability I can be written as

$$I \propto |e^{iI_pt_1}e^{iE_kt_1} + e^{iI_pt_2}e^{i[E_kt_2-\Delta\varphi]}|^2, \tag{13}$$

where $\Delta\varphi = \varphi_1 - \varphi_2$. According to Eq. (13), the ionization yield is modulated by both the ionization potential and the electron momentum. The laser field we use is one-cycle pulses, so the electrons are mainly emitted at the peak of the laser field where $\mathbf{A}(t) \approx 0$. According to the purely classical model [22], the influence of the atomic potential is neglected, so $\mathbf{p} = -\mathbf{A}(t_i)$. When the relative phase between the pulses is 0, we can assume that the two electrons wave packets that can interference are generated at the same vector potential of the two pulses, so $t_2 = t_1 + T_d$. We choose a representative case where $E_k \approx 0$ to examine. Equation (13) can then be simplified as

$$I \propto |e^{iI_pt_1} + e^{i[I_pt_2-\Delta\varphi]}|^2 = 2 + 2\cos(I_pT_d - \Delta\varphi), \tag{14}$$

which explicitly indicates that the modulation period of the ionization yield is $2\pi/I_p$.

When the relative phase is π in Fig. 6(b), the modulation period is nearly the same for the results of the SFA and TDSE, but the envelope of the amplitude variation is quite different.

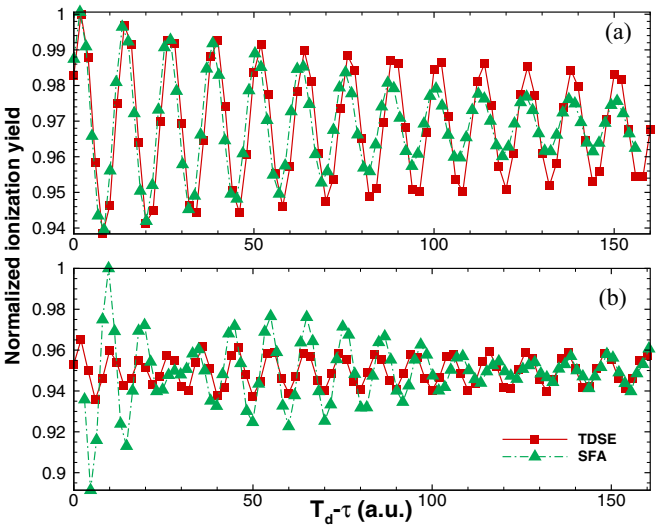

FIG. 6. (Color online) Comparison of normalized ionization yields for the Yukawa potential at 1200 nm, calculated respectively by the TDSE and SFA methods. The total ionization yield is shown, with the relative phase being (a) $\Phi_{\mathrm{CEP}} = 0$ and (b) $\Phi_{\mathrm{CEP}} = \pi$.

In this case, the interference time interval is not equal to T_{d}. The modulation becomes more complex, which is beyond our model.

C. Ionization modulation in the one-multicycle-pulse case

As the ionization modulation is the result of interference of electron wave packets generated by two time-delayed pulses, we can extend the electron wave packet interference from two single-cycle pulses to one multicycle pulse. For a multicycle pulse, the electron wave packets generated at each cycle of the laser field can interference with each other. We expect that the ionization yield can be modulated by varying the wavelength.

To verify our assumption, we use an eight-cycle IR pulse with the wavelength varying from 980 to 1068 nm at a peak intensity of 2×10^{14} W/cm^2. The corresponding Keldysh parameter varies from 0.62 to 0.56. For comparison, we have done the calculations for both the Yukawa potential and the Coulomb potential. The results are shown in Fig. 7. The ionization probability oscillates as a function of the wavelength and there are five identifiable peaks in the range of our calculations. The peak positions are quite close to each other for the Yukawa potential and the Coulomb potential.

We can also attribute the modulation to the result of wave packet interferences between the subpeaks of the laser pulse. However, the difference from the two-pulse time-delay case is that there exists an electric field during the time delay between the two-subpeak ionization. Due to the Stark shift [28], the ionization potential is changed to I_{p}'. According to Eq. (13), the ionization probability should be changed to

$$I \propto |e^{iI_{\mathrm{p}}'t_1} e^{iE_{\mathrm{k}}t_1} + e^{iI_{\mathrm{p}}'t_2} e^{i[E_{\mathrm{k}}t_2 - \Delta\varphi(\lambda)]}|^2, \qquad (15)$$

where $\Delta\varphi$ is a function of the wavelength; for a different wavelength the shift is also different. If we consider the

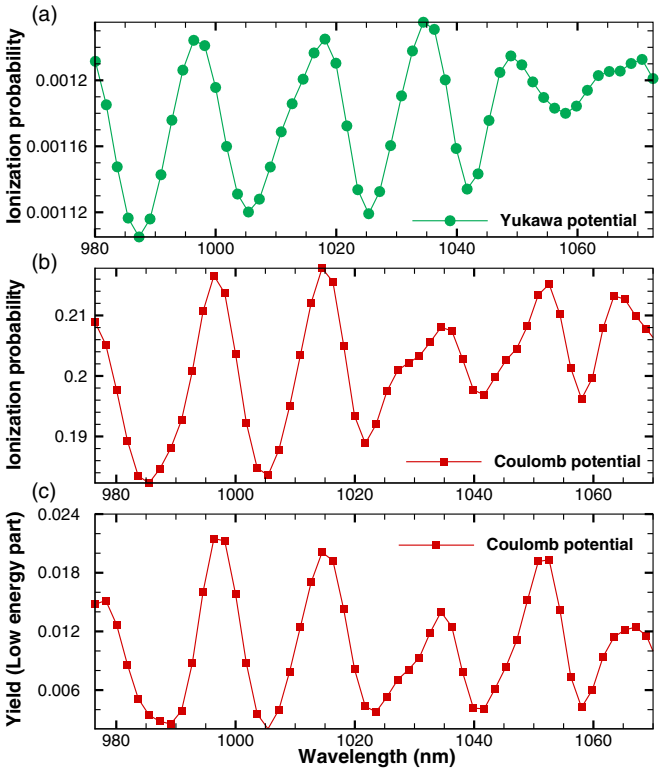

FIG. 7. (Color online) Modulation of the ionization yield as a function of the wavelength for an eight-cycle $\sin^2$ laser pulse calculated by the TDSE with the Coulomb potential and the Yukawa potential, respectively. The peak intensity of laser pulse is fixed at 2×10^{14} W/cm^2. Results are shown for the (a) Yukawa potential and (b) Coulomb potential. (c) Also shown is the very-low-energy (0.01–0.02 a.u.) yield for the Coulomb potential case.

ponderomotive potential U_{p}, where $U_{\mathrm{p}} = E_0^2/4\omega^2$ and E_0 is the field amplitude, the ionization potential with a Stark shift ($I_{\mathrm{p}}' = I_{\mathrm{p}} + U_{\mathrm{p}}$) increases with the wavelength. We find that when I_{p}'/ω is an integer, a maximum of the ionization yield will appear if we neglect the term of $\Delta\varphi(\lambda)$ in Eq. (15). The integer numbers at this laser peak intensity for the range of our calculated wavelength are 25, 26, 27, 28, 29, and 30 and the corresponding wavelengths are 982, 1000, 1018, 1034, 1050, and 1067 nm. The peak positions are roughly at the corresponding wavelengths in Fig. 7, but there are still some discrepancies. Equation (15) shows that the modulation period is also affected by E_{k} and $\Delta\varphi(\lambda)$ in addition to I_{p}'. In Fig. 7(c) we calculate the very-low-energy ionization yield, which is from 0.01 to 0.02 a.u., and the peak positions are the same as those of the total ionization yield in Fig. 7(b). In this way, we can attribute this gap to $\Delta\varphi$, which stems from the phase change of the electron wave packet in the laser field.

In brief, the ionization modulation can also be achieved by varying the wavelength in one laser pulse in the tunneling regime. The underlying physical mechanism is related to the electron wave packet interferences generated in the subcycles and to the Stark shifted ionization potential changing with the wavelength.

IV. SUMMARY

We have theoretically investigated the ionization modulation of H using a pair of identical time-delayed one-cycle IR pulses in the tunneling regime. The TDSE results using the Coulomb potential show more complexity than those of the Yukawa potential because of the existence of the Rydberg state excitation. As we increase the wavelength, the modulation of ionization yield with the Coulomb potential is more regular and gradually approaches the modulation pattern of the Yukawa potential case. Our numerical results and analysis show that the ionization modulation is due to the interference of electron wave packets in the continuum states. We also extend the modulation of ionization yield to the one-multicycle-pulse case by varying the wavelength and find that the ionization modulation also exists due to the interference of electron wave packets generated in different subcycles of the laser pulse.

ACKNOWLEDGMENTS

This work was partially supported by the National Natural Science Foundation of China under Grants No. 11322437, No. 11174016, and No. 11134001; by the National Program on Key Basic Research Project (973 Program) under Grant No. 2013CB922402; and by Program for New Century Excellent Talents in University. The computational results were obtained by using the computer cluster MESO in the State Key Laboratory for Mesoscopic Physics at Peking University.

[1] A. H. Zewail, J. Phys. Chem. A **104**, 5660 (2000).
[2] S. A. Rice and M. Zhao, *Optimal Control of Molecular Dynamics* (Wiley-Interscience, New York, 2000).
[3] M. Shapiro and P. Brumer, *Principles of the Quantum Control of Molecular Processes* (Wiley, Hoboken, 2003).
[4] H. Rabitz, R. de Vivie-Riedle, M. Motzkus, and K. Kompa, Science **288**, 824 (2000).
[5] A. M. Weiner, Rev. Sci. Instrum. **71**, 1929 (2000).
[6] L.-Y. Peng, W.-C. Jiang, J.-W. Geng, W.-H. Xiong, and Q. Gong, Phys. Rep. **575**, 1 (2015).
[7] V. Blanchet, C. Nicole, M.-A. Bouchene, and B. Girard, Phys. Rev. Lett. **78**, 2716 (1997).
[8] D. Meshulach and Y. Silberberg, Nature (London) **396**, 239 (1998).
[9] D. Meshulach and Y. Silberberg, Phys. Rev. A **60**, 1287 (1999).
[10] A. Präkelt, M. Wollenhaupt, C. Sarpe-Tudoran, and T. Baumert, Phys. Rev. A **70**, 063407 (2004).
[11] N. Dudovich, B. Dayan, S. M. Gallagher Faeder, and Y. Silberberg, Phys. Rev. Lett. **86**, 47 (2001).
[12] M. Wollenhaupt, V. Engel, and T. Baumert, Annu. Rev. Phys. Chem. **56**, 25 (2005).
[13] S. X. Hu and A. F. Starace, Phys. Rev. A **68**, 043407 (2003).
[14] M. Wollenhaupt *et al.*, Phys. Rev. Lett. **89**, 173001 (2002).
[15] Y. Gontier and M. Trahin, J. Phys. B **22**, 2531 (1989).
[16] L. V. Keldysh, Zh. Eksp. Teor. Fiz. **47**, 1945 (1964).
[17] R. R. Jones, C. S. Raman, D. W. Schumacher, and P. H. Bucksbaum, *Proceedings of the XIth International Conference on Laser Spectroscopy*, AIP Conf. Proc. No. 290 (AIP, New York, 1993), p. 319.
[18] A. D. Kondorskiy and L. P. Presnyakov, Proc. SPIE **5228**, 394 (2003).
[19] L.-Y. Peng, E. A. Pronin, and A. F. Starace, New J. Phys. **10**, 025030 (2008).
[20] M. H. Xu, L.-Y. Peng, Z. Zhang, Q. H. Gong, X. M. Tong, E. A. Pronin, and A. F. Starace, Phys. Rev. Lett. **107**, 183001 (2011).
[21] S. N. Song, J. W. Geng, H. B. Jiang, and L.-Y. Peng, Phys. Rev. A **89**, 053411 (2014).
[22] W. Becker, F. Grasbon, R. Kopold, D. B. Milošević, G. G. Paulus, and H. Walther, Adv. At. Mol. Opt. Phys. **48**, 35 (2002).
[23] D. B. Milošević, G. G. Paulus, D. Bauer, and W. Becker, J. Phys. B **39**, R203 (2006).
[24] J. Yuan, M. Li, X. Sun, Q. Gong, and Y. Liu, J. Phys. B **47**, 015003 (2014).
[25] W. C. Jiang, W. H. Xiong, T. S. Zhu, L.-Y. Peng, and Q. H. Gong, J. Phys. B **47**, 091001 (2014).
[26] C. H. Lu, S. Zhang, and Z. Sun, Chin. Phys. Lett. **30**, 113302 (2013).
[27] C. H. Lu, S. Zhang, T. Q. Jia, J. R. Qiu, and Z. R. Sun, J. Nonlinear Opt. Phys. Mater. **22**, 1350008 (2013).
[28] H. Rottke, B. Wolff-Rottke, D. Feldmann, K. H. Welge, M. Dörr, R. M. Potvliege, and R. Shakeshaft, Phys. Rev. A **49**, 4837 (1994).